Role of surface plasmon polaritons on optical transmission through double layer metallic hole arrays

R. Ortuño,* C. García-Meca, F. J. Rodríguez-Fortuño, J. Martí, and Alejandro Martínez
Valencia Nanophotonics Technology Center, Universidad Politécnica de Valencia, Campus del Camino de Vera, 46022 Valencia, Spain
(Received 28 August 2008; revised manuscript received 14 November 2008; published 12 February 2009)

We study analytically and numerically the far-field extraordinary optical transmission (EOT) through double-layer metallic grating structures patterned with subwavelength hole arrays. In addition to EOT phenomena due to the well-known surface plasmon polaritons (SPPs) on the outer surfaces such as those on a single layer hole array, further EOT peaks are observed. The separation between the metallic layers is small enough to allow SPPs propagating through the inner interfaces to couple and form an internal SPP, with a different dispersion relation from the outer one and so giving rise to EOT peaks at different frequencies. We propose a relatively simple model to predict the frequencies of those EOT peaks. Internal SPPs show certain unique properties different from the external SPPs: they can give rise to a magnetic response and a negative effective permeability, and the transmission of their EOT peaks increases when no direct line of sight is allowed through the structure. All these findings may be utilized in wavelength tuning of extraordinary optical transmission in subwavelength optics.

DOI: 10.1103/PhysRevB.79.075425 PACS number(s): 73.20.Mf, 71.36.+c, 78.66.Bz, 42.79.Dj

I. INTRODUCTION

A surface plasmon polariton (SPP) is an electromagnetic surface wave traveling along the interface separating a dielectric and a metal. It is produced by the interaction of collective oscillations of free electrons in the metal surface with the electromagnetic wave impinging on the metal. The first theoretical description of surface plasmons dates back to 1957 when Ritchie[1] predicted the existence of surface plasmons when he discussed the plasma losses in thin films. However, it was in 1998, when Ebbesen *et al.*[2] published their pioneering work about extraordinary optical transmission (EOT) through hole arrays in metallic films, when SPPs attracted the attention of fundamental research giving rise to the field of plasmonics. Since then, other studies have proved the existence of EOT, mostly on single-layer metal films with periodic hole arrays, being well accepted that the EOT through single-layer hole arrays originates from the grating coupling between the dispersion relation of the SPPs that propagate along a smooth infinite metal-dielectric interface and the momentum of the incident light taking into account the lattice structure provided by the holes. However, this procedure has to be considered as an approximation due to the fact that it models the momentum of the SPPs on a hole array using the expression of SPPs on a smooth metal-dielectric interface, thus ignoring the effect which the holes may have on the SPP propagation. Nevertheless the predictions of this model are usually very accurate.[3–6]

Though theoretical modeling of multilayers was studied by Economou[7] and following experiments by Kovacs,[8] EOT studies have been focused traditionally on single-layer structures. It is until quite recently when studies of multilayer hole arrays have gained more attention. In this way, transmission through double-layer smooth surfaces[9] or drilled with hole arrays with isotropic[10,11] as well as anisotropic[12] shapes have been studied. Also, the electromagnetic responses of double-layer metal structures perforated with an array of slits[13,14] and near-field optical images of double-layer nanoparticles[15] have been explored. Multilayer structures have also been studied[16] showing, in addition, a left-handed behavior when stacking subwavelength hole array plates.[17]

It is known that when two metal layers are placed closer than the SPP attenuation length, the SPPs that propagate along each of the two inner interfaces couple to each other, thus creating a mode called internal SPPs whose dispersion relation differs from the usual aforementioned dispersion relation of the SPPs on a single interface. Thus, EOT peaks are observed at frequencies different from those expected using the model of SPPs on a single metal-dielectric interface.

In this work, we study both analytically and numerically a structure composed of a dielectric layer sandwiched between two metal layers nanostructured with subwavelength hole arrays. Comparing our work with previous results, we emphasize that we have developed a simple approximate model, in analogy with the model for single-layer hole arrays, to predict analytically an approximate frequency for *all* the EOT peaks coming from the excitation of SPPs on a double-layer hole array structure. To this end, we consider, in analogy with the model for single-layer hole arrays, the dispersion relation of the SPPs propagating on a multilayer structure without holes and equate it with the momentum of the incident light taking into account the periodicity of the structure provided by the holes.

In the simulations we vary various parameters such as the dielectric thickness and its permittivity to study its influence in the transmission spectra. A good agreement between the wavelengths at which EOT occur in simulations and those expected from the calculated SPP dispersion relation via grating coupling is found. From the dispersion relation of the SPPs propagating on a multilayer structure without holes, it can be seen that two types of resonances, internal and external SPPs, are responsible for the EOT. The internal SPP resonates in the inner surfaces of the metal layers, whereas the external SPP resonates in the outer surfaces of the metal layers.

From a different perspective, the field of plasmonics has been in close relation with that of metamaterials. In fact, SPP resonances are responsible for achieving negative index of refraction in metallic metamaterials at optical wavelengths.[18] As it will be shown, we also present that the internal SPPs that our model predicts on a double layer hole array play a fundamental role in achieving a negative effective permeability behavior as the electromagnetic (EM) field forms a virtual current loop between the two metallic layers. These plasmonic resonances are thus sometimes called *LC* resonances[19–22] and are used for achieving negative permeability in metamaterials such as the fishnet.[19–23] The realization of metamaterials at optical wavelengths holds the promise for novel and exciting applications such as superlenses,[24] hyperlenses,[25] or cloaking devices.[26]

Finally, the influence of the alignment of the metallic hole arrays on EOT is also studied. In some configurations, the lateral displacement between the metallic hole arrays permits no direct line of sight through the structure. Nonetheless, the transmission remains remarkably large at resonance. The numerical results show the important role of the EM field in the transmission behavior of the SPP resonances. The structure presented here is of significant importance to the aforementioned applications, especially at optical and terahertz radiation, because smooth interfaces can be realized in the layered structures using modern growth techniques[27] and has potential applications in subwavelength photolithography, near-field microscopy, wavelength-tunable filters, optical modulators, solar selective surfaces, and directional radiation, among others.

The paper is structured as follows: in Sec. II the double-layer metallic structure as well as the system used to analytically obtain the SPP dispersion relation is described. In Sec. III the numerical analysis of the double-layer metallic hole array structure is carried out. A discussion of the structure parameters' influence on the transmission is presented. Finally, some conclusions are given in Sec. IV.

II. DESCRIPTION AND MODEL OF THE DOUBLE-LAYER METALLIC HOLE ARRAY

In this work we consider the role of SPPs in the transmission through a dielectric layer sandwiched between two metallic hole arrays. In order to elucidate the general properties of SPPs on a double-layer metallic hole array, we can calculate the dispersion relation for the SPPs propagating on the multilayer geometry without holes depicted in Fig. 1. The desired dispersion relation has been previously calculated,[7] but we extend it to the general case in which all the layers have an arbitrary electric permittivity ε_i.

Similarly to the case of a partially filled waveguide, the EM fields considered here are referred to as longitudinal section magnetic (LSM_z) where the subscript z refers to the direction which is perpendicular to the interface.[28] These hybrid modes are also named as TM_z. The choice of this kind of EM modes is simply for convenience to satisfy the boundary conditions at the different interfaces. TE modes are not considered as it is widely known that for common media, SPPs only exist for TM polarization.[29]

FIG. 1. (Color online) Geometry of a five-layer system formed by a dielectric film (thickness d, permittivity ε_d) sandwiched between two metal layers (thickness h, permittivity ε_{m1} and ε_{m2}) and surrounded by two semi-infinite dielectric layers (permittivities ε_1 and ε_2).

In order to derive the expressions of the EM fields we begin by defining a proper expression for the magnetic and electric vector potentials called $\vec{A}$ and $\vec{F}$, respectively. It is known[28] that it is sufficient to let $\vec{A}$ have a unique component in the direction in which the fields are desired to be TM when deriving the field expressions that are TM to a given direction, independently of the coordinate system. The remaining components of $\vec{A}$ as well as all of $\vec{F}$ are set equal to zero.

As Fig. 1 shows, without loss of generality, we let the layers be parallel to the x axis so for simplicity a one-dimensional problem is assumed. Therefore $\varepsilon=\varepsilon(z)$ depends only on one spatial coordinate as the layers are considered infinite in the y direction. To calculate the dispersion relation of the structure we consider the waves propagating along the x direction of a Cartesian coordinate system, showing no spatial variation in the perpendicular, out-of-plane y direction. Moreover we seek solutions with an evanescent decay in the z direction normal to the interfaces, i.e., we look for propagating wave solutions confined to the interfaces. Having all this in mind, $\vec{A}$, which must satisfy the Helmholtz equation, can be described as $\vec{A}=A_z\hat{z}=Af(z)e^{i\beta x}\hat{z}$. The function $f(z)=e^{k_z z}$ describes the depth dependence of the EM fields. In general, $k_z=\pm\sqrt{\beta^2-k_0^2\varepsilon}$ with both plus and minus signs admissible. However, only one value of k_z is allowed, corresponding to the solution that approaches zero when $z\rightarrow\pm\infty$. β is called the propagation constant of the traveling waves and corresponds to the component of the wave vector in the direction of propagation. Once A_z is found, the next step is to find the EM field components via[28]

$$E_x=-j\frac{1}{\varpi\mu\varepsilon}\frac{\partial^2 A_z}{\partial x\,\partial z},\quad H_x=0, \tag{1}$$

$$E_y=0,\quad H_y=-\frac{1}{\mu}\frac{\partial A_z}{\partial x}, \tag{2}$$

$$E_z = -j\frac{1}{\varpi\mu\varepsilon}\left(\frac{\partial^2}{\partial z^2} + k_0^2\varepsilon\right)A_z, \quad H_z = 0, \tag{3}$$

where the homogeneity in the y direction ($\partial/\partial y = 0$) has been taken into account. Using the equation set (1)–(3) in all layers yields

$$H_y = -j\frac{\beta}{\mu}Ae^{-k_1 z}e^{j\beta x}, \tag{4a}$$

$$E_x = -\frac{\beta k_1}{\varpi\mu\varepsilon_0\varepsilon_1}Ae^{-k_1 z}e^{j\beta x}, \tag{4b}$$

$$E_z = -j\frac{\beta^2}{\varpi\mu\varepsilon_0\varepsilon_1}Ae^{-k_1 z}e^{j\beta x} \tag{4c}$$

for $z > d/2 + h$;

$$H_y = -j\frac{\beta}{\mu}Be^{-k_2 z}e^{j\beta x} - j\frac{\beta}{\mu}Ce^{k_2 z}e^{j\beta x}, \tag{5a}$$

$$E_x = -\frac{\beta k_2}{\varpi\mu\varepsilon_0\varepsilon_{m1}}Be^{-k_2 z}e^{j\beta x} + \frac{\beta k_2}{\varpi\mu\varepsilon_0\varepsilon_{m1}}Ce^{k_2 z}e^{j\beta x}, \tag{5b}$$

$$E_z = -j\frac{\beta^2}{\varpi\mu\varepsilon_0\varepsilon_{m1}}Be^{-k_2 z}e^{j\beta x} - j\frac{\beta^2}{\varpi\mu\varepsilon_0\varepsilon_{m1}}Ce^{k_2 z}e^{j\beta x} \tag{5c}$$

for $d/2 < z < d/2 + h$;

$$H_y = -j\frac{\beta}{\mu}De^{-k_3 z}e^{j\beta x} - j\frac{\beta}{\mu}Ee^{k_3 z}e^{j\beta x}, \tag{6a}$$

$$E_x = -\frac{\beta k_3}{\varpi\mu\varepsilon_0\varepsilon_d}De^{-k_3 z}e^{j\beta x} + \frac{\beta k_3}{\varpi\mu\varepsilon_0\varepsilon_d}Ee^{k_3 z}e^{j\beta x}, \tag{6b}$$

$$E_z = -j\frac{\beta^2}{\varpi\mu\varepsilon_0\varepsilon_d}De^{-k_3 z}e^{j\beta x} - j\frac{\beta^2}{\varpi\mu\varepsilon_0\varepsilon_d}Ee^{k_3 z}e^{j\beta x} \tag{6c}$$

for $-d/2 < z < d/2$;

$$H_y = -j\frac{\beta}{\mu}Fe^{-k_4 z}e^{j\beta x} - j\frac{\beta}{\mu}Ge^{k_4 z}e^{j\beta x}, \tag{7a}$$

$$E_x = -\frac{\beta k_4}{\varpi\mu\varepsilon_0\varepsilon_{m2}}Fe^{-k_4 z}e^{j\beta x} + \frac{\beta k_4}{\varpi\mu\varepsilon_0\varepsilon_{m2}}Ge^{k_4 z}e^{j\beta x}, \tag{7b}$$

$$E_z = -j\frac{\beta^2}{\varpi\mu\varepsilon_0\varepsilon_{m2}}Fe^{-k_4 z}e^{j\beta x} - j\frac{\beta^2}{\varpi\mu\varepsilon_0\varepsilon_{m2}}Ge^{k_4 z}e^{j\beta x} \tag{7c}$$

for $(-d/2 + h) < z < -d/2$; and

$$H_y = -j\frac{\beta}{\mu}He^{k_5 z}e^{j\beta x}, \tag{8a}$$

$$E_x = \frac{\beta k_5}{\varpi\mu\varepsilon_0\varepsilon_2}He^{k_5 z}e^{j\beta x}, \tag{8b}$$

$$E_z = -j\frac{\beta^2}{\varpi\mu\varepsilon_0\varepsilon_2}He^{k_5 z}e^{j\beta x} \tag{8c}$$

for $z < -(d/2 + h)$, where $k_i = k_{zi}$ is the component of the wave vector perpendicular to the interface. In the central regions the modes localized at the interfaces couple due to the fact that the separation between the layers is small enough to allow coupling of the evanescent fields, as can be seen in the equations. Finally, the dispersion relation is obtained by solving the linear equation system enforcing the continuity of the tangential EM components at every interface separating two media which yields an implicit expression for β and ϖ via

$$\frac{\left(\frac{k_2}{\varepsilon_{m1}} - \frac{k_3}{\varepsilon_d}\right)\left(\frac{k_1}{\varepsilon_1} + \frac{k_2}{\varepsilon_{m1}}\right)e^{k_2 h}e^{-k_3 d/2} + \left(\frac{k_2}{\varepsilon_{m1}} + \frac{k_3}{\varepsilon_d}\right)\left(\frac{k_1}{\varepsilon_1} - \frac{k_2}{\varepsilon_{m1}}\right)e^{-k_2 h}e^{-k_3 d/2}}{\left(\frac{k_2}{\varepsilon_{m1}} + \frac{k_3}{\varepsilon_d}\right)\left(\frac{k_1}{\varepsilon_1} + \frac{k_2}{\varepsilon_m}\right)e^{k_2 h}e^{k_3 d/2} + \left(\frac{k_2}{\varepsilon_{m1}} - \frac{k_3}{\varepsilon_d}\right)\left(\frac{k_1}{\varepsilon_1} - \frac{k_2}{\varepsilon_{m1}}\right)e^{-k_2 h}e^{k_3 d/2}}$$

$$- \frac{\left(\frac{k_4}{\varepsilon_{m2}} - \frac{k_3}{\varepsilon_d}\right)\left(\frac{k_5}{\varepsilon_2} - \frac{k_4}{\varepsilon_{m2}}\right)e^{-k_4 h}e^{k_3 d/2} + \left(\frac{k_4}{\varepsilon_{m2}} + \frac{k_3}{\varepsilon_d}\right)\left(\frac{k_4}{\varepsilon_{m2}} + \frac{k_5}{\varepsilon_2}\right)e^{k_4 h}e^{k_3 d/2}}{\left(\frac{k_4}{\varepsilon_{m2}} + \frac{k_3}{\varepsilon_d}\right)\left(\frac{k_5}{\varepsilon_2} - \frac{k_4}{\varepsilon_{m2}}\right)e^{-k_4 h}e^{-k_3 d/2} + \left(\frac{k_4}{\varepsilon_{m2}} - \frac{k_3}{\varepsilon_d}\right)\left(\frac{k_4}{\varepsilon_{m1}} + \frac{k_5}{\varepsilon_2}\right)e^{k_4 h}e^{-k_3 d/2}} = 0. \tag{9}$$

For the sake of simplicity, we limit ourselves to the symmetric case in which both the semi-infinite layers' relative dielectric constants are equal to $\varepsilon_1 = \varepsilon_2 = \varepsilon_{\text{air}}$ and $\varepsilon_{m1} = \varepsilon_{m2} = \varepsilon_{\text{Cr}}$, where Cr stands for chromium modeled with a Drude dispersion.[30] The results presented here are easily extensible for other types of metal.

The SPPs dispersion relation $\beta(\varpi)$ given by Eq. (9) accounts for two types of SPP modes decoupled from each other, namely, the internal SPP and the external SPP which propagate along the internal and the external metal-dielectric interfaces, respectively.[7]

For our modeling of double layer hole arrays, we take

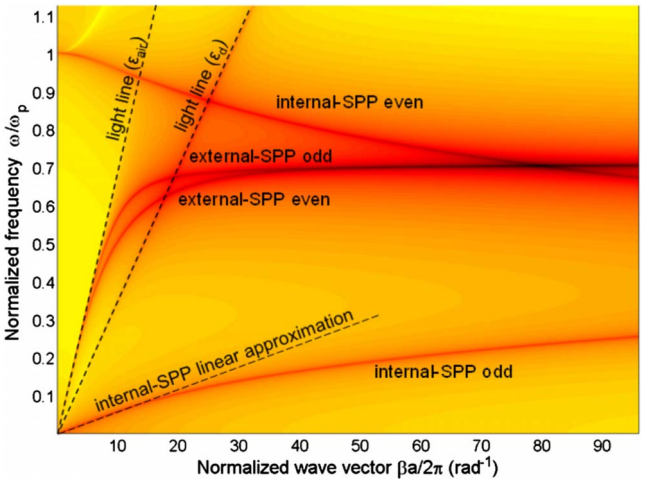

FIG. 2. (Color online) Dispersion relation of SPPs at a dielectric (d=4 nm and ε_d=4) sandwiched between Drude double-metal layers (h=45 nm) surrounded by air.

Eq. (9) as a starting point, as it describes the fundamentals of SPPs in smooth double-layer metallic structure interfaces. However, in analogy to what is done for single-layer structures, we can consider that the SPP dispersion relation on a double-layer hole array will be similar to that obtained in the smooth double-layer metallic structure. This procedure allows us to predict analytically all the EOT peaks coming from the excitation of both internal- and external-SPP modes at those wavelengths at which they couple to the incoming light via grating coupling on a double-layer hole array structure. However, this model is clearly an approximation, since it does not take into account the effect of the holes on the SPP dispersion relation.

In a metal film with a periodic square array of holes, the interaction between light and the SPP obeys momentum and energy conservation given by[2]

$$|\vec{k}_{spp}| = |\vec{k}_x + \vec{G}_{i,j}| = |\vec{k}_0 \sin\phi + i\vec{G}_x + j\vec{G}_y|, \tag{10}$$

where $|\vec{k}_{spp}| \equiv \beta(\varpi)$ is the wave vector of the SPP derived from Eq. (9), $\vec{k}_0 \sin\phi$ is the in-plane component of the incident wave vector, $\vec{G}_x$ and $\vec{G}_y$ are the reciprocal lattice vectors where for a square array have the same value $|\vec{G}_x| = |\vec{G}_y| = 2\pi/a$, a being the lattice periodicity and i,j are both integers.

The dispersion relation given by Eq. (9), with h=45 nm, d=4 nm and ε_d=4, is represented in Fig. 2 in a purely real $\beta - \varpi$ plane, thus neglecting the imaginary part of the solution which does not affect our modeling of the resonant frequencies. The internal and external-SPPs dispersion curves can be seen, with odd and even symmetric modal fields with respect to the x axis due to the symmetry of the structure.[6,7,29] The light lines are trivial solutions for our problem and correspond to the case when all fields are zero.[7]

For large wave vectors the frequency of the SPP tends to the characteristic SPP frequency[29]

$$\varpi_{sp} = \frac{\varpi_p}{\sqrt{\varepsilon_\infty + \varepsilon_i}}, \tag{11}$$

with $\varepsilon_i = \varepsilon_d$ or ε_{air} for internal or external SPPs, respectively. This trend supports the interpretation of internal and external SPP modes. In the opposite regime of short wave vectors $\beta \ll k_p$, corresponding to low frequencies, the SPP propagation constant related to internal SPPs can be described according to the linear approximation

$$\beta^{int} \equiv |\vec{k}_{sp}^{int}| = |\vec{k}_o|\sqrt{\varepsilon_d}\left[\frac{d}{d + \lambda_p \coth(k_p h)/\pi}\right]^{-1/2}, \tag{12}$$

which is an extension of that presented in Ref. 7, where $k_p = 2\pi/\lambda_p = \varpi_p/c$. Regarding the external SPP curves, for the same frequency range, they can be described by

$$\beta^{ext} \equiv |\vec{k}_{sp}^{ext}| = |\vec{k}_o|\sqrt{\frac{\varepsilon_{air}\varepsilon_m}{\varepsilon_{air} + \varepsilon_m}}, \tag{13}$$

where it has been considered that in this frequency range the odd and even external SPPs are close enough to be represented by the same expression.

It can be seen that, as the dielectric thickness d decreases, the internal-SPP mode lowers in frequency due to an increased coupling between the SPPs at the two internal interfaces. On the other hand, as it is expected, the external SPP is very close to the light line of the cladding, i.e., $\beta^{ext} \approx |\vec{k}_o|$, which does not vary with d.

The straightforward analytical expressions (12) and (13) can be substituted into Eq. (10) to analytically predict the approximate excitation frequencies at which the incoming light couples to both the internal and external SPPs on a double layer hole array via grating coupling. As can be seen, when applying Eq. (10), several modes (i,j) will appear for both internal and external SPPs, accounting for all the EOT peaks arising from SPPs in the double-layer hole array. Indeed, this model permits a complete identification, classification, and enumeration of such peaks.

III. NUMERICAL RESULTS

Once the dispersion relation is known, we perform numerical simulations by using the commercial software CST Microwave Studio, a general-purpose EM simulator based on the finite integration technique (FIT), to investigate the transmission through the double-metallic layers and its dependence with the parameters of the sandwiched dielectric. As depicted in Fig. 3 the structure lies on the xy plane and consists of a dielectric layer of variable thickness d, and permittivity ε_d, sandwiched between two chromium metal layers of thickness h nanostructured with subwavelength circular hole arrays filled with air. The surrounding medium is also considered to be air. The incoming wave is considered to be normal to the structure with the $\vec{E}$ field polarized along the x axis. The metal layers' parameters ε_∞=1, ϖ_p=6.7034 $\times 10^{15}$ rad/s, and γ=1.138$\times 10^{13}$ Hz for the Drude model are extracted from Ref. 31. The thickness of the metal h =100 nm, the radius of the hole r=800 nm, and the lattice parameter a=3990 nm are kept constant in all the simula-

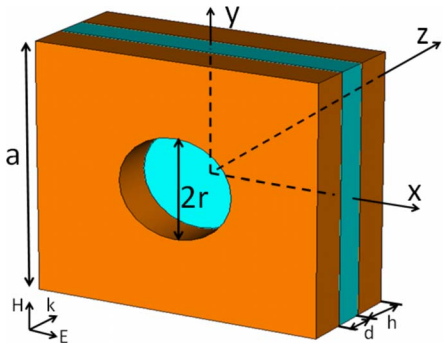

FIG. 3. (Color online) Schematic diagram of the double-metallic layer hole array unit cell. The unit cell structural parameters are labeled: period a, hole radius r, metal thickness h, and dielectric separation d.

tions. The dielectric thickness d and permittivity ε_d will be varied throughout the study. Unit cell boundary conditions are applied for in-plane boundaries representing an infinite-periodic structure, and open boundaries are considered in the perpendicular direction.

The normalized transmission spectrum together with the dispersion relation given by Eq. (9) for a dielectric thickness $d=300$ nm is depicted in Fig. 4 for both (a) $\varepsilon_d=1$ and (b) $\varepsilon_d=4$. The predicted EOT peak frequencies calculated by equating the matching condition given by Eq. (10) with the full dispersion relation of Eq. (9) (solid lines) are shown for different values of (i,j) of both internal and external SPPs. The predicted frequencies are seen to approximately match the simulated spectra EOT peaks (dashed lines). Agreement between simulation and our model is not perfect, in the same way as in a single-layer hole array, because the dispersion relation of the SPPs used as matching condition does not take into account the presence of the holes, which cause scattering losses and a resonance shift. As a consequence, the predicted resonant frequencies are slightly larger than those obtained in simulations.[4] Although not indicated, the multiple small peaks seen in Fig. 4 at high frequencies can each be accurately associated with a certain (i,j) resonance of either internal or external SPPs.

On the other hand, the transmission minima are the result of Wood's anomaly.[32] The dotted lines in Fig. 4 highlight the position of Wood's anomalies for different (i,j). It can be seen how the expected Wood's anomalies positions are in a good agreement with the minima positions of the simulated spectra.

We will now analyze in detail the features of the EM fields in each peak and confirm their agreement with the model. We will start by analyzing the external-SPP resonances. Two main peaks for the external SPP appear in the simulated frequency range, which correspond to the first- and second-order transmission resonances according to Eqs. (10) and (13) when $(i,j)=(1,0)$ and (1,1), respectively. Note that, when $\varepsilon_d=4$, the simulated spectra show two distinct separate peaks corresponding to the odd and even symmetric (1,0) external-SPP modes, while the dispersion relation used by the model predicts a single hybridized frequency for both. This is because the external SPPs on opposite interfaces experience increased coupling through the holes, which the

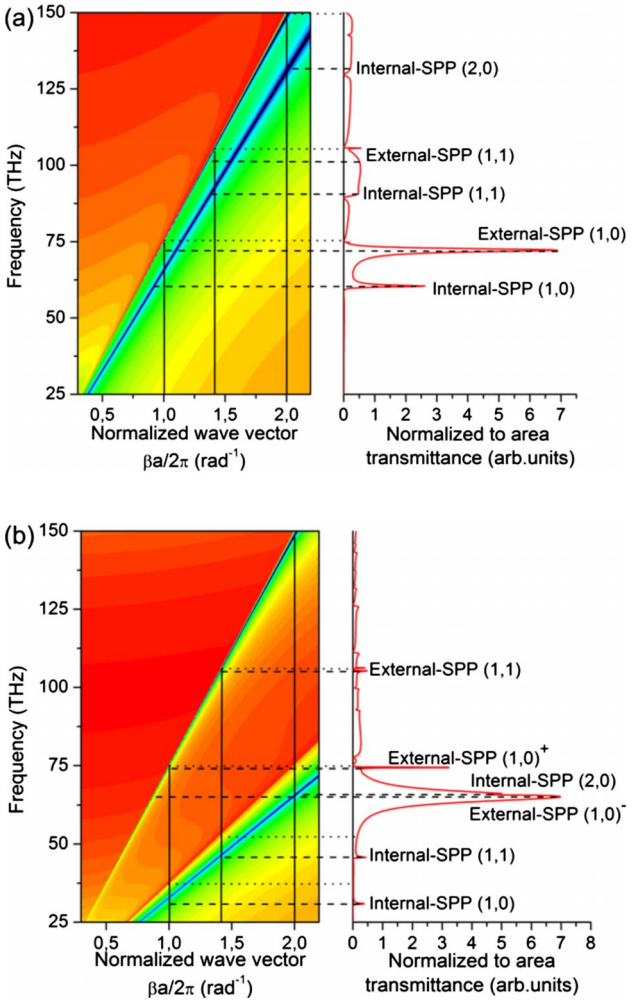

FIG. 4. (Color online) Representation of the dispersion relation (left) and the calculated normalized transmission (right) for (a) $\varepsilon_d=1$ and (b) $\varepsilon_d=4$. In both cases $d=300$ nm. The solid lines represent the position at which the matching grating conditions are fulfilled. The simulated EOT peak frequencies are shown with dashed lines. The dotted lines highlight the expected position of Wood's anomalies. The subscripts + and − stand for odd and even symmetry modes, respectively.

model does not take into account. Figure 5 shows the mode profiles of the first-order external-SPP resonances for both $\varepsilon_d=1$ and 4 when $d=300$ nm. It can be seen that the external-SPP EM fields are located on the outer metal-air interfaces, being particularly concentrated at the edge of the holes. Also note that for the case $\varepsilon_d=4$, the (1,0) external resonances are very close in frequency to an internal resonance, which explains why SPPs can also be seen in the inner dielectric layer.

We now analyze the internal-SPP resonances. Several EOT peaks owing to internal SPPs are seen and indicated in Fig. 4. The EM field profiles for the first and second internal-SPP modes are plotted in Fig. 6, both for $\varepsilon_d=1$ and 4. These EM field patterns fully match our predictions. The EM fields are clearly concentrated on the internal dielectric layer, as expected for an internal-SPP resonance. Also, the different modes (i,j) show the expected wavelike features in the transversal direction.

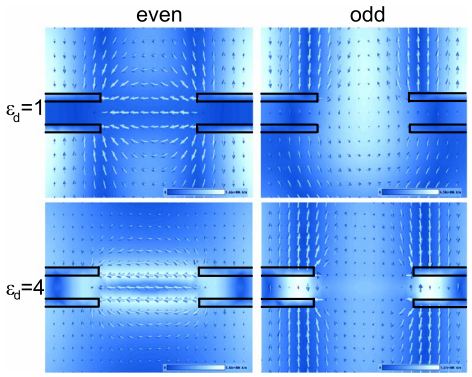

FIG. 5. (Color online) EM field distribution for even (left) and odd (right) external-SPP resonance at xz plane for $d=300$ nm and $\varepsilon_d=1$ (top) and $\varepsilon_d=4$ (down). The arrows represent the E field; the color scale represents $|H|$ and points out of the page. Blue (gray) and white colors display zero and maximum values of the amplitude of the magnetic field, respectively. The black lines are a guide for the eyes enclosing the metallic layers.

The internal SPPs show in general less transmission than the external SPPs as they are concentrated inside optically thick metallic layers which increase the attenuation due to the absorption of the metal layer. The external SPPs peaks show high transmission, as the EM field is concentrated at the edges of the holes and the transmission is achieved by tunneling through them.[3,33]

As intuitively expected, the inner dielectric permittivity affects the internal-SPP dispersion relation while the outer dielectric determines the external-SPP dispersion relation. By

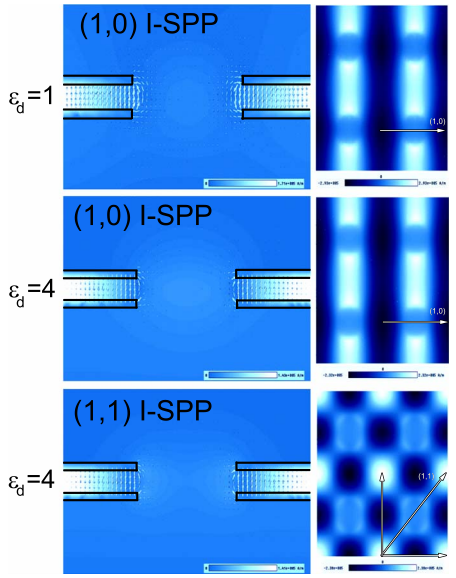

FIG. 6. (Color online) EM field distribution at (1,0) (top and middle) and (1,1) (down) internal-SPP resonance for $d=300$ nm and $\varepsilon_d=1$ (top) and $\varepsilon_d=4$ (middle and down). (Left) The E field is represented by arrows; the color scale represents $|H|$ at xz plane. The black lines are a guide for the eyes enclosing the metallic layers. (Right) H_y distribution maps in the xy plane. Dark blue (black), blue (gray), and white colors display minimum, zero, and maximum values of the amplitude of the magnetic field, respectively.

increasing the inner dielectric permittivity, the dispersion relation of the internal SPP shifts down in frequency, reducing its slope by a factor $\varepsilon_d^{1/2}$. The external SPP is unaffected by the inner dielectric, except for some considerations which we study later. This behavior is in good agreement with simulations.

Moreover, the dielectric permittivities can be adjusted to excite the external- and internal-SPP modes of different orders (i,j) at the same frequency overlapping its transmission maxima, as it is almost the case for the even external (1,0) and internal (2,0) SPP modes when $\varepsilon_d=4$ [see Fig. 4(b)], thus forming a single peak in which the resulting EM field has a (2,0) pattern in the inner dielectric layer and a (1,0) pattern in the claddings.

Also it should be noticed how the transmission for both the internal and external SPPs decreases when the inner dielectric permittivity ε_d differs from that of the surrounding claddings. This behavior is similar to that of a single metal layer when the claddings surrounding the metal are different, so that decreased coupling of the SPP sustained in each metal-dielectric interface is allowed giving rise to a decrease in transmission.[16,33,34]

Taking into account the subwavelength thickness of the structure, we retrieved from the transmitted and reflected spectra the effective constituent parameters of the structure[35] shown in Fig. 7 for the cases when dielectric permittivity is $\varepsilon_d=1$ and 4 and $d=300$ nm. It can be seen that the retrieved ε_{eff} is negative below the first external-SPP EOT peak, while μ_{eff} becomes negative at the internal-SPP resonances. This magnetic negative response can be explained looking at the current and field distribution for the internal-SPP modes. Antiparallel currents are excited at opposite internal metallic interfaces, closed by an electric displacement current. Thus, a virtual current loop (VCL) between the metallic layers on a perpendicular plane to the incoming magnetic field will be formed giving rise to a magnetic resonant response of negative μ_{eff}.[36] If the internal-SPP resonances occur below the external-SPP resonance, negative ε_{eff} and μ_{eff} coincide in frequency and a negative effective index n_{eff} is retrieved, thus, achieving an EOT with a negative effective index nature.[37] This was indeed the case with our simulations. The internal-SPP resonances have been sometimes called LC resonances due to their analogy to a LC circuit.[19–22] The presented dispersion relation of internal SPPs is consistent with the LC model: an increase in ε_d lowers the resonant frequency, while an increase in d increases the resonant frequency. From the internal-SPP dispersion curve Eq. (12) and the matching condition Eq. (10) we can derive an expression, similar to that presented in Ref. 20, linking the resonant frequency at which an internal SPP is excited with the frequency ϖ_{LC} of the LC equivalent circuit of the VCL,

$$\lambda_{i,j}^{\text{int}} = \frac{2\pi}{|\vec{G}_{i,j}|}\sqrt{\varepsilon_d}\left[\frac{d}{d+\lambda_p \coth(k_p h)/\pi}\right]^{-1/2} = \frac{2\pi c}{|\vec{G}_{i,j}|}\left(\frac{1}{\varpi_{LC}}\right). \tag{14}$$

Regarding the extracted parameters, the external-SPPs resonances do not show magnetic response because the displacement current does not form a VCL with the electric current

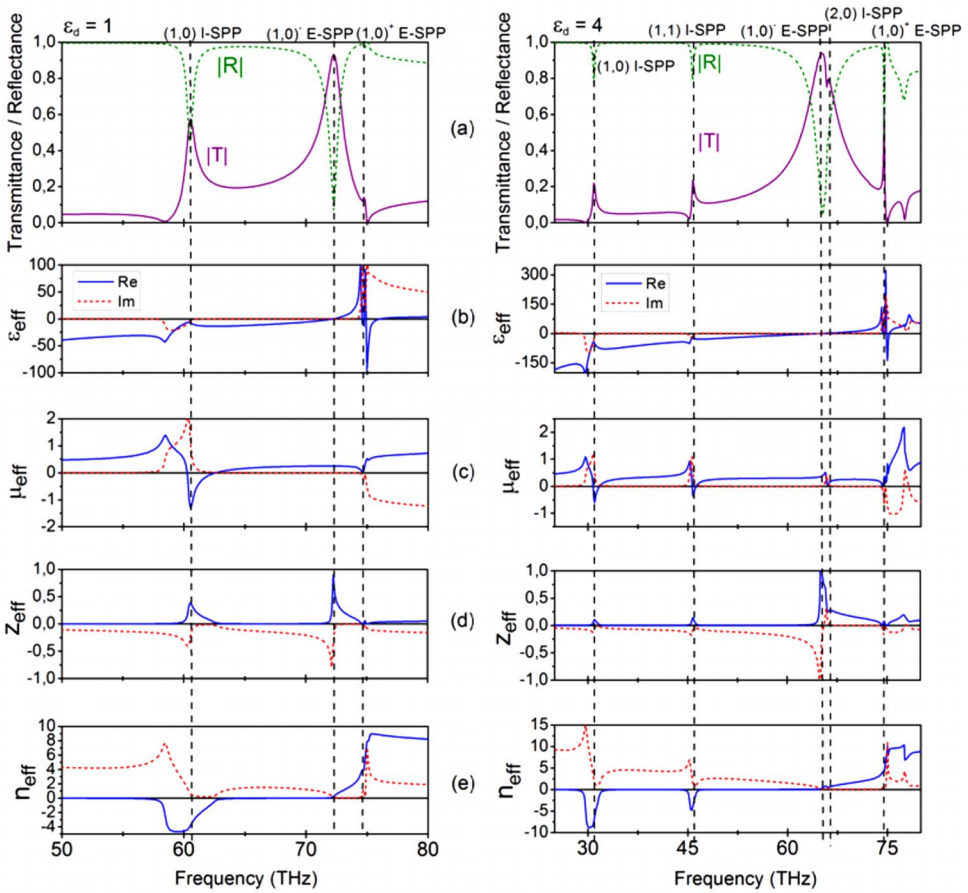

FIG. 7. (Color online) Transmission and reflection spectrum (a) and retrieved parameters of the structure: effective values of permittivity ε_{eff}, permeability μ_{eff}, impedance Z_{eff}, and refractive index n_{eff} are depicted in (b), (c), (d), and (e), respectively, for $\varepsilon_d=1$ (left) and $\varepsilon_d=4$ (right). The dashed lines indicate the position of the resonant frequencies of the internal-SPP (I-SPP) and external-SPP (E-SPP) for different (i,j) values.

as the E field is not concentrated between the plates but at the rims of the holes (see Fig. 5), rather their effect is to change the negative ε_{eff} typical for metallic composites at low frequencies into a positive ε_{eff}, as required by the matching condition between ε_{eff} and μ_{eff} ($Z_{\text{eff}}\approx 1$) for a high transmission peak, where μ_{eff} is known to be small and positive. However, for the antisymmetric external SPP a magnetic response is excited due to the fact that considerable E_z remains between the metallic layers as to build the VCL.[21]

The presented relationship between the internal-SPP EOT peaks and its resonant negative magnetic response μ_{eff} in double-layer hole array is, in fact, a very appropriate way of modeling the well-known fishnet metamaterial whose structure is fundamentally the same as that presented here.[19–23] In fact, in previous results the resonant magnetic response of the fishnet structure was simply termed a magnetic plasmon polariton (MPP)[20–22] without further indication of its real physical origin. We now give this resonance a complete interpretation as the (1,0) internal-SPP mode. The same is true for higher order internal-SPPs modes usually termed high order MPPs,[20,21] which with the presented model can be clearly identified and enumerated.

Now we will study the effect of varying the dielectric thicknesses d as shown in Fig. 8. The transmission for the external SPP decreases slightly as d grows.[11] On the other hand, the transmission of the internal SPP rises with d. As predicted by the model [Eqs. (12) and (13)] and confirmed by simulations [see Fig. 8(a)], a change in the inner dielectric thickness shifts the internal-SPP resonance while not affecting the external SPP, as it was previously stated. However, as shown in Fig. 8(b), the external SPP shifts in frequency for varying d if ε_d is different to that of the claddings. This external-SPP frequency shift with d is not predicted by our model, as it considers smooth metal layers without holes, such that the external SPPs propagate entirely in the outer metal-air interfaces and so do not depend on the inner dielectric parameters. However, if one looks at the simulated EM field distribution of the external SPPs on the real hole array (see Fig. 5), it can be seen that the EM field is concentrated at the edges of the holes, and so the external SPPs *do* interact with the internal dielectric medium, due to its lack of holes, leading to a downshift of their resonant frequency. The interaction is greater for thicker internal dielectric layers. Nevertheless, we can adjust the presented model taking this into account by using an appropriately chosen equivalent-permittivity ε_{eq}, instead of the permittivity of the claddings, ε_{air}, so that Eq. (13) matches the simulated EOT frequencies. In this way, the interaction of the external SPPs with the inner dielectric due to the presence of the holes is being introduced in our hole-free model as an equivalent outer dielectric.[16] Thus, ε_{eq} will depend both on the external air and the internal dielectric at the holes, equaling ε_{air} in the case of $d=0$, and increasing toward an average value between the cladding and dielectric permittivities as d increases, as shown in Fig. 9. In that way, if $\varepsilon_d=1$, ε_{eq} remains constant and close to ε_{air}, so no resonant frequency variation is observed with d.

Up until now we have considered the hole arrays drilled only in the metal layers with a lack of holes in the inner

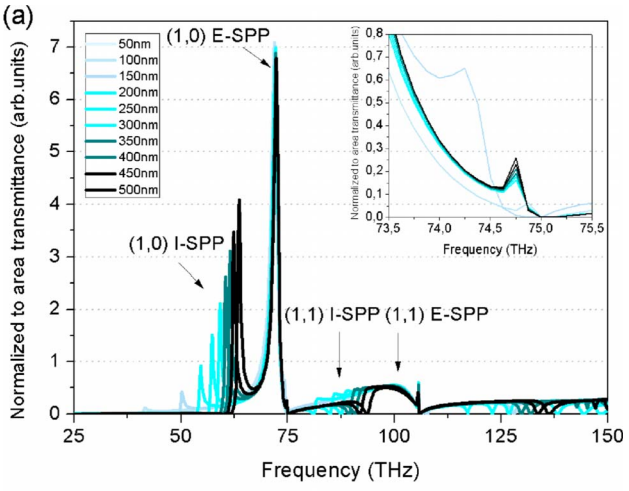

FIG. 8. (Color online) Normalized-to-area transmittance for different dielectric thickness d and dielectric permittivity ε_d. (a) $\varepsilon_d=1$ and (b) $\varepsilon_d=4$. The insets of both figures show the odd external-SPP resonance. The arrows mark the position of the internal-SPP (I-SPP) and external-SPP (E-SPP) for different resonances (i,j).

dielectric. However, in the case that the dielectric layer had holes aligned with those in the metal layers, then the previously discussed external-SPP resonance shift with d does not take place (not shown), suggesting that $\varepsilon_{\mathrm{eq}}$ remains equal to $\varepsilon_{\mathrm{air}}$ when holes are milled in the dielectric. The line of circles of Fig. 9 shows this case when $\varepsilon_d=4$. This supports the interpretation that the frequency dependence of the external SPPs with the inner dielectric arises due to the external-SPP EM fields entering the inner layers through the holes. Taking all this into account, we conclude that the suitable value for the equivalent-permittivity $\varepsilon_{\mathrm{eq}}$, which depends on the thickness d and dielectric permittivity ε_d, is highly determined by the structure design and its related EM field distribution. This behavior could be a means of tuning the external EOT peaks.

Finally, the influence of the alignment between the holes on the spectrum transmission is also studied. The metallic layers were displaced with respect to each other a distance of a/m, with m ranging from 1 (perfect alignment) to 6, along the reciprocal directions ΓX and ΓM of the reduced Brillouin zone, though only the transmission spectrums achieved with

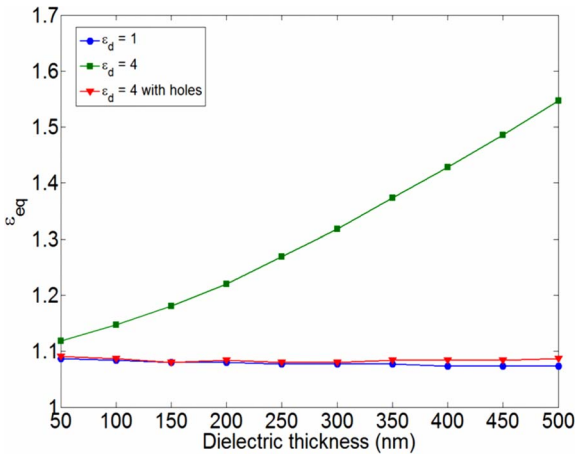

FIG. 9. (Color online) Variation of $\varepsilon_{\mathrm{eq}}$ vs d for different ε_d values.

$m=2$, 3, and 4 are depicted in Fig. 10. We will study the case of $d=300$ nm and $\varepsilon_d=1$. We find that the transmission, which depends strongly on the alignment of the holes, remains remarkably large at resonance, even though in some configurations the displacement of the two metal layers permits no direct line of sight through the structure. Moreover, the internal-SPP resonances, not only maintain, but rather increase their transmission compared with the aligned case and exceed, in most of the cases, the transmission of the external-SPP resonances, which show reduced transmission than in the aligned case. When the lateral shift between the two layers is close to half the grating period ($m=2$) a maximum transmission is reached for the internal SPPs, further decreasing with m. This has been explained by the matching of the Poynting vector between the layers.[10] However, we have noticed that the conclusions of Ref. 10 apply only to the internal SPPs but not to the external SPPs, due to the low confinement of the EM field between the layers, so the amount of transmission for the external SPPs is practically unaffected with the lateral displacement. Also, two additional

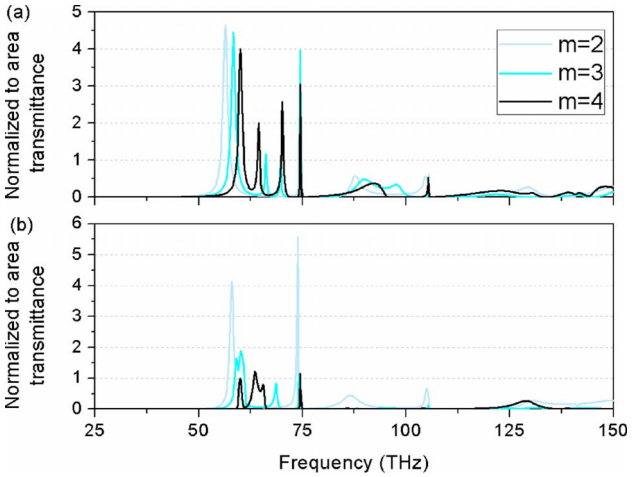

FIG. 10. (Color online) Transmission for samples with lateral shifts of $a/2$ [light blue (light gray)], $a/3$ [blue (gray)], and $a/4$ (black) respectively, between the two metal layers for $d=300$ nm and $\varepsilon_d=1$ for ΓX (a) and ΓM (b) directions.

peaks appear in the spectrum.[10] These peaks, likewise the ordinary EOT peaks, do not arise from neither Fabry-Perot resonances between two metallic layers, because the dielectric thickness embedded in the metal layers is much smaller than the wavelength of resonance, nor from propagating diffractive orders emerging from the metal layers by the normally incident light, because the period of the grating is smaller than the wavelength resonance.[14]

IV. CONCLUSIONS

We have obtained analytically the dispersion relation of SPPs in a double-layer metallic structure and shown by numerical analysis that light coupling to the external and internal SPPs originates EOT. A good matching between the theoretical and simulated resonant frequencies is observed. Moreover, the strong influence of the sandwiched dielectric layer parameters in the transmission resonances is presented. These effects can be used to tune the resonant frequencies for both the internal and external SPPs. In addition, at the internal-SPP resonant frequencies a negative effective permeability is achieved as a VCL is formed between the metallic layers which can be used to design negative-index metamaterials. The influence of the alignment between holes was also studied. Even in the case of no direct line of sight through the structure, the transmission remained remarkably large at resonances. The model presented here surely facilitates the interpretation and design of double-layer structures.

The transmission features through double-layer subwavelength metallic hole arrays open up a new dimension in the design and operation of plasmonics devices. Understanding the coupling of evanescent waves in complex double-layer metallic hole arrays nanostructures is of fundamental interest and practical importance in designing optical devices that could become important building blocks in future nanooptical systems.

ACKNOWLEDGMENTS

Financial support by the Spanish MCyT and EU-FEDER under Contract No. TEC2005-06923-C03-03 is gratefully acknowledged. R.O., C.G.-M., and F.J.R.-F. also acknowledge financial support from grants FPI of Universidad Politécnica de Valencia, FPU of MICINN and from a grant of La Caixa, respectively.

*ruormo@ntc.upv.es

[1] R. H. Ritchie, Phys. Rev. **106**, 874 (1957).
[2] T. W. Ebbesen, H. J. Lezec, H. F. Ghaemi, T. Thio, and P. A. Wolf, Nature (London) **391**, 667 (1998).
[3] L. Martín-Moreno, F. J. García-Vidal, H. J. Lezec, K. M. Pellerin, T. Thio, J. B. Pendry, and T. W. Ebbesen, Phys. Rev. Lett. **86**, 1114 (2001).
[4] C. Genet and T. W. Ebbesen, Nature (London) **445**, 39 (2007).
[5] D. E. Grupp, H. J. Lezec, T. W. Ebbesen, K. M. Pellerin, and T. Thio, Appl. Phys. Lett. **77**, 1569 (2000); T. Thio, H. F. Ghaemi, H. J. Lezec, P. A. Wolff, and T. W. Ebbesen, J. Opt. Soc. Am. B **16**, 1743 (1999); A. Degiron, H. J. Lezec, W. Barnes, and T. W. Ebbesen, Appl. Phys. Lett. **81**, 4327 (2002); H. F. Ghaemi, T. Thio, D. E. Grupp, T. W. Ebbesen, and H. J. Lezec, Phys. Rev. B **58**, 6779 (1998).
[6] H. Raether, *Surface Plasmons on Smooth and Rough Surfaces and on Gratings*, Springer Tracts in Modern Physics Vol. 111 (Springer-Verlag, Berlin, 1988).
[7] E. N. Economou, Phys. Rev. **182**, 539 (1969).
[8] G. J. Kovacs and G. D. Scott, Phys. Rev. B **16**, 1297 (1977).
[9] Y. Wang, Appl. Phys. Lett. **82**, 4385 (2003).
[10] F. Miyamaru and M. Hangyo, Phys. Rev. B **71**, 165408 (2005).
[11] Y. H. Ye and J. Y. Zhang, Opt. Lett. **30**, 1521 (2005).
[12] H. Li, S. Xie, R. Zhou, Q. Liu, X. Zhou, and M. Yuan, J. Phys.: Condens. Matter **20**, 415223 (2008).
[13] A. P. Hibbins, J. R. Sambles, C. R. Lawrence, and J. R. Brown, Phys. Rev. Lett. **92**, 143904 (2004).
[14] H. B. Chan, Z. Marcet, K. Woo, D. B. Tanner, D. W. Carr, J. E. Bower, R. A. Cirelli, E. Ferry, F. Klemens, J. Miner, C. S. Pai, and J. A. Taylor, Opt. Lett. **31**, 516 (2006).
[15] R. M. Bakker, V. P. Drachev, H. K. Yuan, and V. M. Shalaev, Opt. Express **12**, 3701 (2004).
[16] Z. H. Tang, R. W. Peng, Z. Wang, X. Wu, Y. J. Bao, Q. J. Wang, Z. J. Zhang, W. H. Sun, and M. Wang, Phys. Rev. B **76**, 195405 (2007).
[17] M. Beruete, M. Sorolla, and I. Campillo, Opt. Express **14**, 5445 (2006); M. Beruete, M. Sorolla, M. Navarro-Cía, F. Falcone, I. Campillo, and V. Lomakin, *ibid.* **15**, 1107 (2007).
[18] V. M. Shalaev, Nat. Photonics **1**, 41 (2007); C. García-Meca, R. Ortuño, R. Salvador, A. Martínez, and J. Martí, Opt. Express **15**, 9320 (2007); F. J. Rodriguez-Fortuño, C. García-Meca, R. Ortuño, J. Martí, and A. Martínez, Phys. Rev. B **79**, 075103 (2009).
[19] S. Zhang, W. Fan, N. C. Panoiu, K. J. Malloy, R. M. Osgood, and S. R. J. Brueck, Phys. Rev. Lett. **95**, 137404 (2005).
[20] T. Li, J. Q. Li, F. M. Wang, Q. J. Wang, H. Liu, S. N. Zhu, and Y. Y. Zhu, Appl. Phys. Lett. **90**, 251112 (2007).
[21] T. Li, H. Liu, F. M. Wang, J. Q. Li, Y. Y. Zhu, and S. N. Zhu, Phys. Rev. E **76**, 016606 (2007).
[22] T. Li, H. Liu, F. M. Wang, Z. G. Dong, S. N. Zhu, and X. Zhang, Opt. Express **14**, 11155 (2006).
[23] S. Zhang, W. Fan, K. J. Malloy, S. R. J. Brueck, N. C. Panoiu, and R. M. Osgood, Opt. Express **13**, 4922 (2005); G. Dolling, C. Enkrich, M. Wegener, C. M. Soukoulis, and S. Linden, Opt. Lett. **31**, 1800 (2006); G. Dolling, C. Enkrich, M. Wegener, C. M. Soukoulis, and S. Linden, Science **312**, 892 (2006).
[24] J. B. Pendry, Phys. Rev. Lett. **85**, 3966 (2000); N. Fang, H. Lee, C. Sun, and X. Zhang, Science **308**, 534 (2005); D. R. Smith, *ibid.* **308**, 502 (2005).
[25] N. Fang, H. Lee, C. Sun, and X. Zhang, Science **308**, 534 (2005); Z. Liu, H. Lee, Y. Xiong, C. Sun, and X. Zhang, *ibid.* **315**, 1686 (2007).
[26] J. B. Pendry, D. Schurig, and D. R. Smith, Science **312**, 1780 (2006); W. Cai, U. K. Chettiar, A. V. Kildishev, and V. M.

Shalaev, Nat. Photonics **1**, 224 (2007).
[27] G. Dehlinger, L. Diehl, U. Gennser, H. Sigg, J. Faist, K. Ensslin, D. Grützmacher, and E. Müller, Science **290**, 2277 (2000).
[28] C. A. Balanis, *Advanced Engineering Electromagnetics* (Wiley, New York, 1989).
[29] S. A. Maier, *Plasmonics: Fundamental and Applications* (Springer, New York, 2007).
[30] P. Drude, Ann. Phys. **306**, 566 (1900).
[31] A. D. Rakic, A. B. Djurisic, J. M. Elazar, and M. L. Majewski, Appl. Opt. **37**, 5271 (1998).
[32] R. W. Wood, Philos. Mag. **4**, 396 (1902); R. W. Wood, Phys. Rev. **48**, 928 (1935).
[33] S. A. Darmanyan and A. V. Zayats, Phys. Rev. B **67**, 035424 (2003).
[34] A. Krishnan, T. Thio, T. J. Kim, H. J. Lezec, T. W. Ebbesen, P. A. Wolff, J. B. Pendry, L. Martín-Moreno, and F. J. Garcia-Vidal, Opt. Commun. **200**, 1 (2001); A. Benabbas, V. Halté, and J. Y. Bigot, Opt. Express **13**, 8730 (2005).
[35] D. R. Smith, D. C. Vier, T. Koschny, and C. M. Soukoulis, Phys. Rev. E **71**, 036617 (2005).
[36] Z. Huang, J. Xue, Y. Hou, J. Chu, and D. H. Zhang, Phys. Rev. B **74**, 193105 (2006).
[37] C. García-Meca, R. Ortuño, F. J. Rodríguez-Fortuño, J. Martí, and A. Martínez, Opt. Express (to be published).